Revealing the origin of the strong second harmonic generation of Li2CdXS4 and Li2CdXS4 (X=Ge or Sn)

A. H. Reshak

Citation: Journal of Applied Physics **119**, 095709 (2016); doi: 10.1063/1.4943100
View online: http://dx.doi.org/10.1063/1.4943100
View Table of Contents: http://scitation.aip.org/content/aip/journal/jap/119/9?ver=pdfcov
Published by the AIP Publishing

Revealing the origin of the strong second harmonic generation of Li_2CdXS_4 and Li_2CdXS_4 (X = Ge or Sn)

A. H. Reshak[a)]
New Technologies - Research Centre, University of West Bohemia, Univerzitni 8, 306 14 Pilsen, Czech Republic and Center of Excellence Geopolymer and Green Technology, School of Material Engineering, University Malaysia Perlis, 01007 Kangar, Perlis, Malaysia

(Received 21 October 2015; accepted 19 February 2016; published online 4 March 2016)

Second harmonic generation (SHG) and the first hyperpolarizability (β_{ijk}) of two novel quaternary diamond-like semiconductors, Li_2CdGeS_4 and Li_2CdSnS_4, are investigated based on the band structure calculations. Calculations show that these materials possess wide and direct energy gaps of about 3.10 eV (Li_2CdGeS_4) and 3.23 eV (Li_2CdSnS_4) in close agreement with the measured gaps (3.15 eV and 3.26 eV). The energy gap values confirm that these materials exhibit exceptional laser damage thresholds. The presence of polarizable M-S bonds tunes these compounds to exhibit strong SHG. The calculated linear optical properties exhibit considerable anisotropy, which favors the enhanced phase matching conditions necessary for observation of SHG and optical parametric oscillation. It has been found that Li_2CdGeS_4 and Li_2CdSnS_4 exhibit negative uniaxial anisotropy and positive birefringence. The calculated SHG of the dominant component is about 18.64 pm/V for Li_2CdGeS_4, which is larger than that obtained from Li_2CdSnS_4 (12.75 pm/V). These results are in concordance with the experimental value of the well known nonlinear crystal $KTiOPO_4$. The calculated first hyperpolarizability (β_{333}) at $\lambda = 1064$ nm is about 13.015×10^{-30} esu for Li_2CdGeS_4 and 9.704×10^{-30} esu for Li_2CdSnS_4. © *2016 AIP Publishing LLC*.
[http://dx.doi.org/10.1063/1.4943100]

I. INTRODUCTION

In recent years, ultra-violet (UV), visible, and infra-red (IR) laser radiation at wavelengths that are presently inaccessible via conventional sources have been in demand for many industrial, medical, biological, and entertainment applications.[1–3] However, it is still desirable to find materials with promising nonlinear optical (NLO) properties. The quest for the development of novel more efficient and compact quantum electronic devices requires a search for design and fabrication of new materials which should be less expensive and more technological, with novel applications.[4,5] These materials can be used as converters, deflectors, and modulators of electromagnetic radiation, for the design and production of light emitting diodes, for more sensitive detectors, and as nonlinear optical materials.[6–8] Recently, two novel quaternary diamond-like semiconductors, Li_2CdGeS_4 and Li_2CdSnS_4,[9–13] were synthesized by Lekse *et al.*[14] It has been found that these materials have a wide band gap, which causes them to have a high laser damage threshold.[14,15] In these materials, the orientation of the tetrahedral building blocks causes these materials to have a non-centrosymmetric structure, resulting in the loss of inversion symmetry which in turn gives a non-zero second harmonic generation (SHG).[16] The presence of polarizable M-S bonds in these materials results in a strong SHG. Therefore, having a high laser damage threshold and strong SHG makes these materials promising candidates for nonlinear applications in the IR region.[14,15]

Much attention has been given to the investigation of the Li_2CdGeS_4 and Li_2CdSnS_4 compounds. Lekse *et al.*[14] have synthesized Li_2CdGeS_4 and Li_2CdSnS_4, investigated their structures and the SHG. Jang *et al.*[17] have reported that Li_2CdGeS_4 is an excellent NLO material with a wide transparency range. Recently, Brant *et al.*[18] have investigated the SHG and the laser damage threshold of Li_2CdGeS_4 and found that the Li_2CdGeS_4 produces strong SHG in the IR region and possesses an exceptional laser damage threshold. Few theoretical calculations using non-full potential methods to calculate the electronic structure and the linear optical properties were reported.[19–21] None of these calculations have reported the SHG of Li_2CdGeS_4 and Li_2CdSnS_4 compounds and the relation between the structure and the resulting NLO properties. Toward this, we have addressed ourselves to performing comprehensive theoretical calculations using the full potential method within different exchange-correlation potentials to reach the maximum accuracy in calculating the band structure and hence the linear and nonlinear optical properties. It is well-known that the accuracy of the results is very sensitive to the selection of the exchange-correlation potential. The theoretical methods of studying the relationship between the structure and the nonlinear optical susceptibilities may be a better solution before venturing into the physical synthesizing of a new material. Unfortunately, the reported SHG measurements for Li_2CdGeS_4 and Li_2CdSnS_4 lack detailed descriptions about the complex second-order nonlinear optical susceptibility tensors; moreover, no information regarding the microscopic first hyperpolarizability (β_{ijk}) for these compounds is available in the literature. The microscopic first

a)Author to whom correspondence should be addressed. Electronic mail: maalidph@yahoo.co.uk

hyperpolarizability term cumulatively yields a bulk observable second order susceptibility term, $\chi^{(2)}_{ijk}(\omega)$, which in turn is responsible for the high SHG response.[22,23] Due to the recent improvement in computational technologies, it has been proven that the first-principles calculation is a strong and useful tool to predict the crystal structure and the properties related to the electron configuration of a material before its synthesis.[24–27]

II. COMPUTATIONAL DETAILS

The influence of replacing Sn by Ge on the electronic band structures and the linear and nonlinear optical susceptibilities were investigated by means of density functional theory (DFT). The all-electron full-potential linearized augmented plane wave plus the local orbitals (FP-LAPW + lo) method as implemented in the WIEN2k package[28] was used to solve the Kohn Sham equations. We have used the minimum radius of the muffin-tin spheres (R_{MT}) values as 2.0 a.u. for all atoms. This value was chosen to insure that there is no charge leakage out of the atomic sphere cores. The crystal structures of Li_2CdGeS_4 and Li_2CdSnS_4 were taken from the x-ray diffraction data (XRD) reported by Lekse *et al.*[14] Using Perdew-Burke-Ernzerhof generalized gradient approximation (PBE-GGA),[29] the crystal structures of Li_2CdGeS_4 and Li_2CdSnS_4 were optimized by minimizing the forces acting on each atom. The relaxed geometries of Li_2CdGeS_4 and Li_2CdSnS_4 compounds were used to calculate the electronic band structures, the density of states, the electronic charge density, and the linear and nonlinear optical susceptibilities using the PBE-GGA and the recently modified Becke-Johnson potential (mBJ).[30] It has been found that the mBJ succeeds by a large amount in bringing the calculated energy gap closer to the experimental one. Therefore, we chose to present the results obtained by mBJ. The mBJ allows the calculation of the band gap with an accuracy similar to very expensive GW calculations. It is a semilocal approximation to an atomic "exact-exchange" potential and a screening term.[30] The following states are considered as valence electrons: ($2s^1$), ($4s^2$ $4p^2$), ($5s^2$ $5p^2$), ($4p^6$ $4d^{10}$ $5s^2$), and ($3s^2$ $3p^4$) for Li, Ge, Sn, Cd, and S, respectively. The crystal structures of Li_2CdGeS_4 and Li_2CdSnS_4 are shown in Fig. 1; from the unit cell, it is clear that during substituting Ge by Sn atoms, the Sn atoms occupied the Cd atoms' positions. To achieve the total energy convergence, the basis functions in the *IR* are expanded up to $R_{MT} \times K_{\max} = 7.0$ and inside the atomic spheres for the wave function. The maximum value of l is taken as $l_{max} = 10$, while the charge density is Fourier

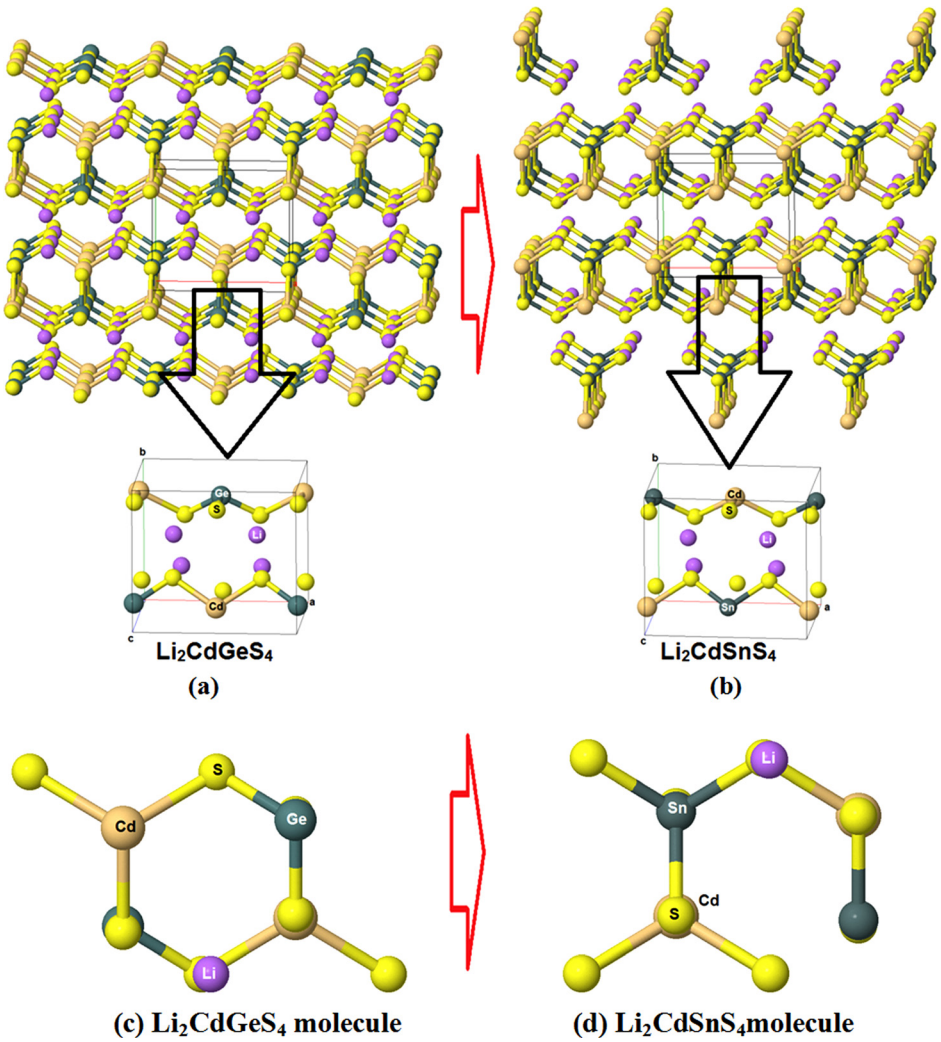

FIG. 1. (a) The crystal structure of Li_2CdGeS_4 along the unit cell. (b) The crystal structure of Li_2CdSnS_4 along the unit cell. (c) Molecule of Li_2CdGeS_4. (d) Molecule of Li_2CdSnS_4.

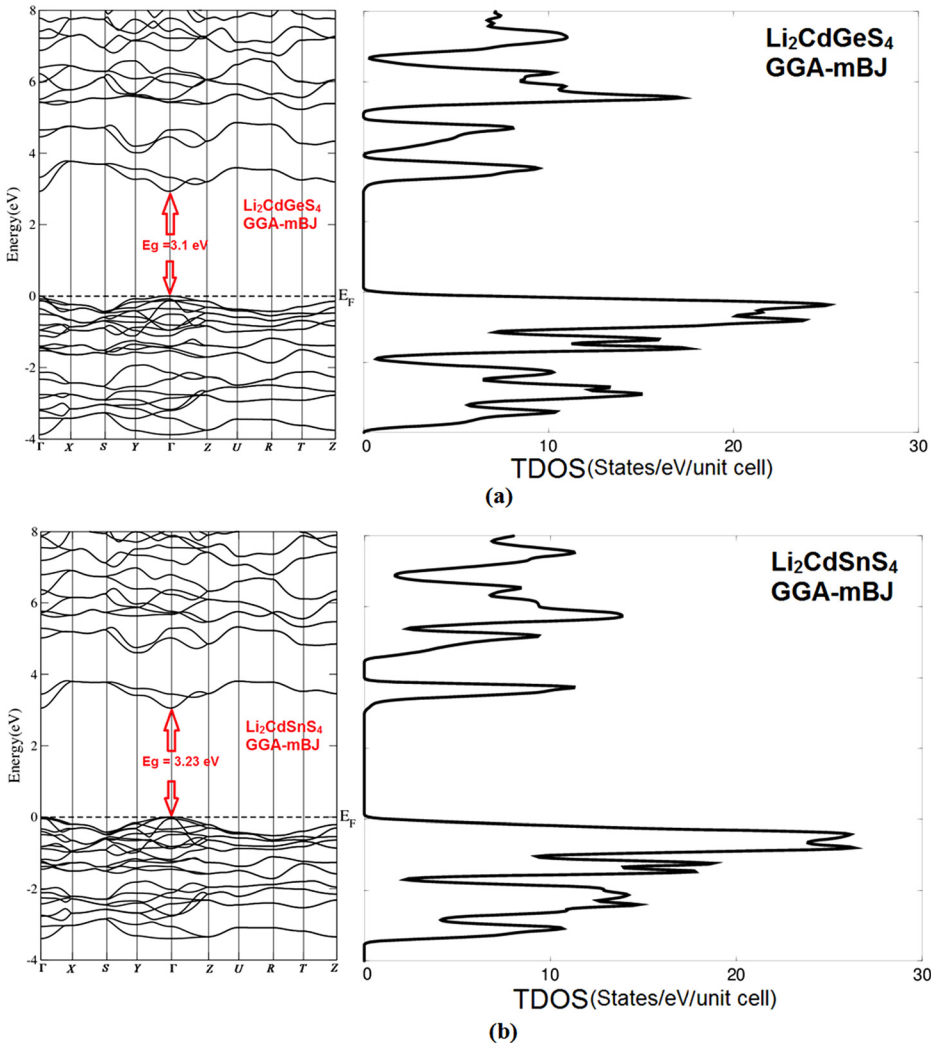

FIG. 2. (a) Calculated electronic band structure along with the calculated total density of states for Li_2CdGeS_4. (b) Calculated electronic band structure along with the calculated total density of states for Li_2CdSnS_4.

expanded up to $G_{max} = 12.0(\text{a.u.})^{-1}$. A self-consistency is obtained using 300 $\vec{k}$ points in the irreducible Brillouin zone (*IBZ*). Since the total energy of the system is stable within 0.00001 Ry, the self-consistent calculations are converged. The calculations of the electronic band structures, the density of states, and the electronic charge density are performed within 1000 $\vec{k}$ points in the *IBZ*, while the linear and nonlinear optical susceptibilities are obtained by using 2000 $\vec{k}$ points in the *IBZ*.

III. RESULTS AND DISCUSSION

A. Electronic band structure and density of states

The calculated electronic band structure along the total density of states (TDOS) for Li_2CdGeS_4 and Li_2CdSnS_4 using mBJ is presented in Figs. 2(a) and 2(b). It has been found that both compounds exhibit a direct band gap (Γ^{VBM}-Γ^{CBM}). The calculated band gaps using mBJ are about 3.10 eV (Li_2CdGeS_4) and 3.23 eV (Li_2CdSnS_4), in good agreement with the measured one (3.15 eV for Li_2CdGeS_4)[14] and (3.26 eV for Li_2CdSnS_4).[14] Therefore, a material with such an energy band gap value is expected to possess a high laser damage threshold.[14,18] The upper valence band and the lower conduction band around Fermi level show a very high k-dispersion. This reflects the high mobility of the carriers. The conduction band minimum (CBM) of Li_2CdGeS_4 (Li_2CdSnS_4) is formed by S-3p and Ge-4s (Sn-5s) orbitals, whereas the valence band maximum (VBM) of both compounds is formed by S-3p orbitals. It is clear that the Cd orbitals exhibit an insignificant contribution to CBM and VBM; thus, the variations in divalent elements can be systematically explored to assess the effects on SHG efficiencies, as well as other attractive properties, while maintaining a wide band gap.[18]

The calculated TDOS confirms the existence of the wide energy gaps and the energy gap values. Furthermore, we have calculated the partial density of states (PDOS) to explore the orbital dispersions and the orbital roles with Ge replaced by Sn, as shown in Figs. 3(a)–3(n). It has been noticed that Ge-4s, Cd-4d, and S1,2,3–3s/3p orbitals exhibit insignificant influence in the matter of peak heights whilst replacing Ge by Sn, as shown in Figs. 3(a) and 3(b). Whereas a significant influence occurs in the matter of peak heights and locations for Ge-4p/4d, Cd-3s/4p, and Li-2s orbitals, as shown in Figs. 3(c) and 3(d). It is interesting to see that the contribution of S1,2,3-atoms is significantly influenced by substituting Ge by Sn (Figs. 3(i) and 3(j)), while Ge-, Cd-, and Li-atoms show only minor changes (Figs. 3(k)–3(n)). Therefore, the sum of all changes exhibits a clear

influence on the bonding character and the optical properties of the Li_2CdSnS_4 compound.

For deep investigation, to explore the influence of substituting Ge by Sn on the electronic structure and hence the resulting properties, we have taken a careful look into the valence electronic charge density distribution, taking into account the Slater covalent radii and the Pauling electronegativity of Li, Cd, Ge, Sn, and S. In Figs. 4(a) and 4(b), we have illustrated the valence electron charge density distribution along the (1 0 1) crystallographic plane. The electronegativity of Li, Cd, Ge, Sn, and S is 0.98, 1.69, 2.01, 1.96, and 2.58, respectively. As we have mentioned, during substituting Ge by Sn, the Sn atoms occupied the Cd atoms' positions; therefore, the electronegativity difference between S and Ge is less than that between S and Cd atoms; thus, the S atom forms a covalent bonding with the Ge atom in Li_2CdGeS_4 (Fig. 4(a)), whereas in Li_2CdSnS_4 the S atom forms mostly an ionic and partially covalent bond with Cd and mostly covalent with the

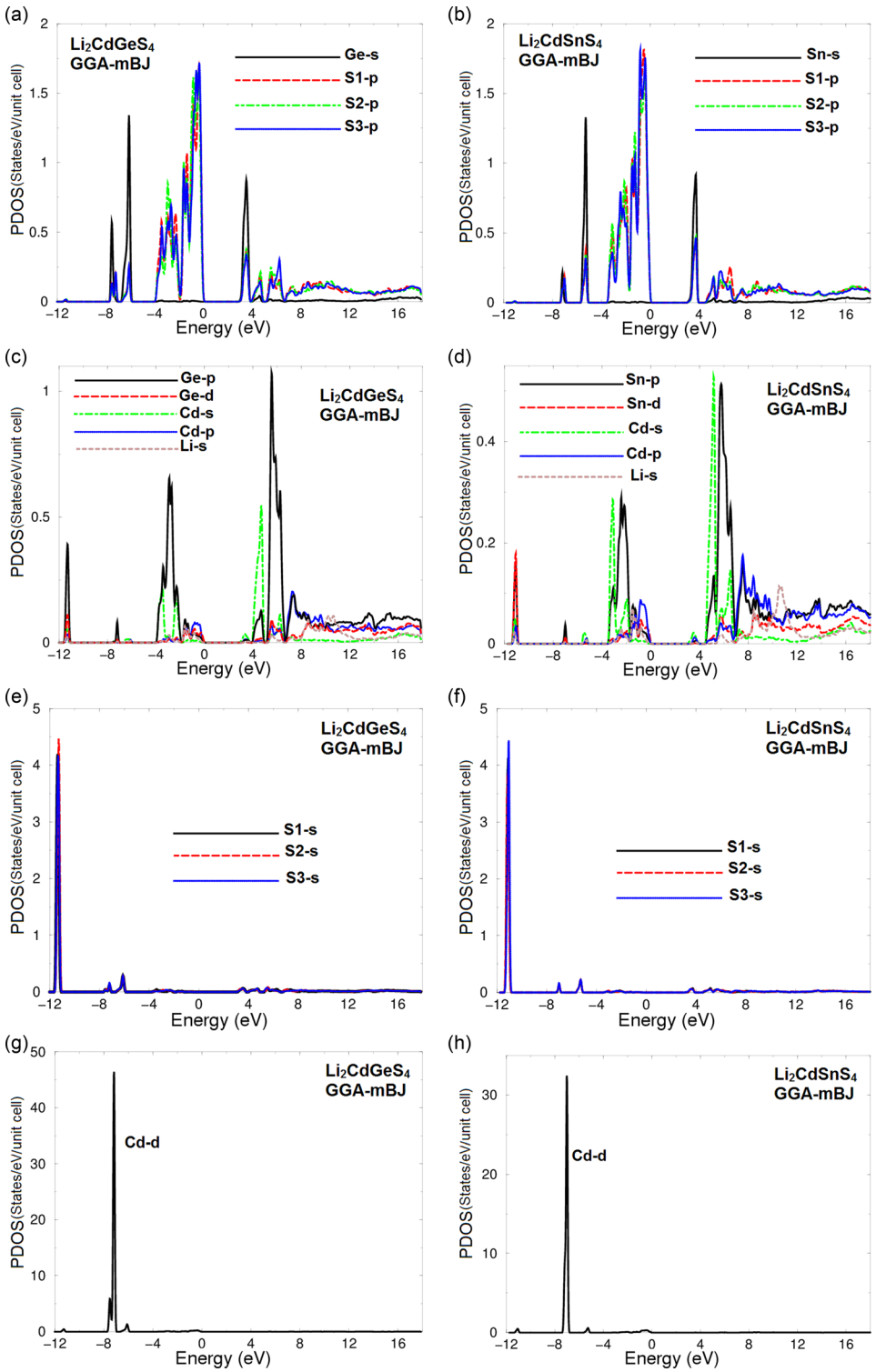

FIG. 3. (a)–(n) Calculated partial density of states for Li_2CdGeS_4 and Li_2CdSnS_4.

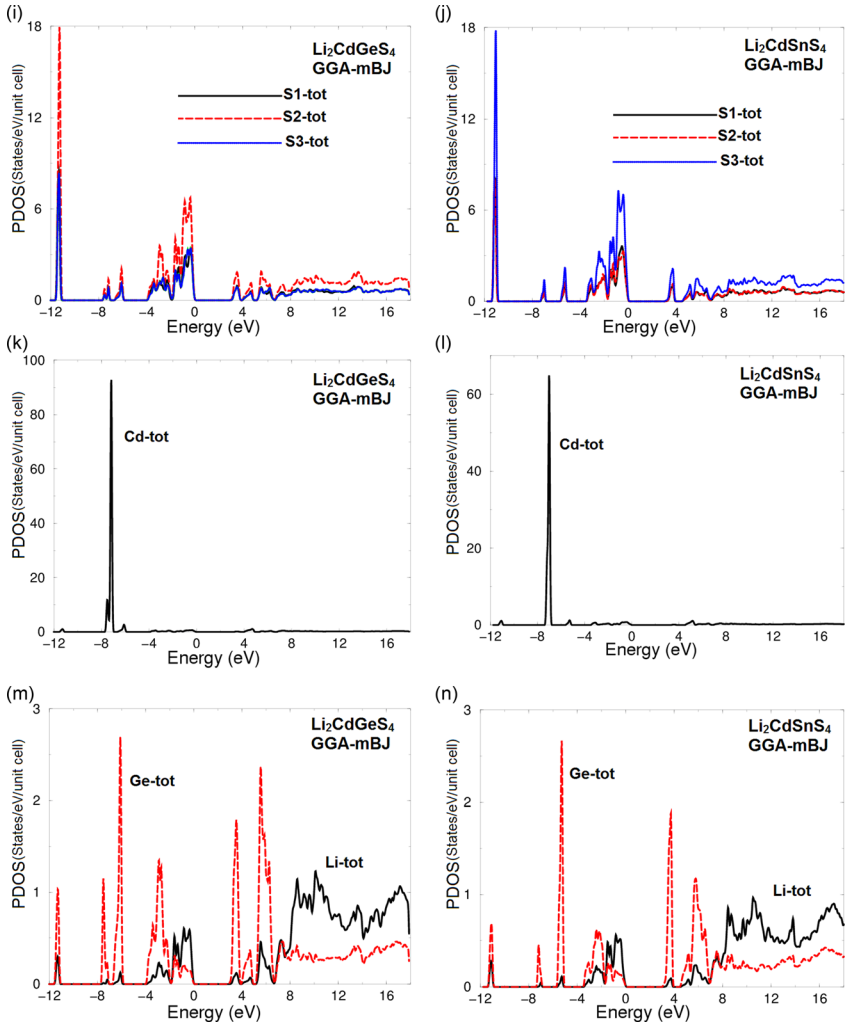

FIG. 3. (*Continued.*)

Sn atom. It has been noticed that the bond between Ge and S atoms leads to perturbation of the contours surrounding S atoms (Fig. 4(a)), while in Cd-S bonding the contours around S and Cd atoms remain uniform (Fig. 4(b)), confirming the dominant ionic nature. These figures bring a clear visualization to understand the origin of the differences in the electronic properties of the two compounds. The covalent bonding is more favorable for the transport of the carriers than the

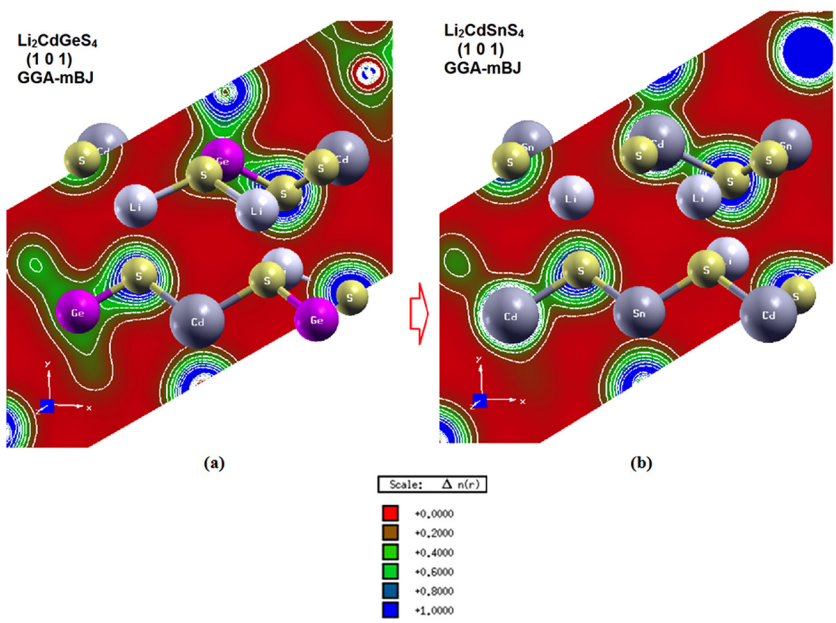

FIG. 4. (a) Calculated valence electronic charge density distribution of Li_2CdGeS_4. (b) Calculated valence electronic charge density distribution of Li_2CdSnS_4.

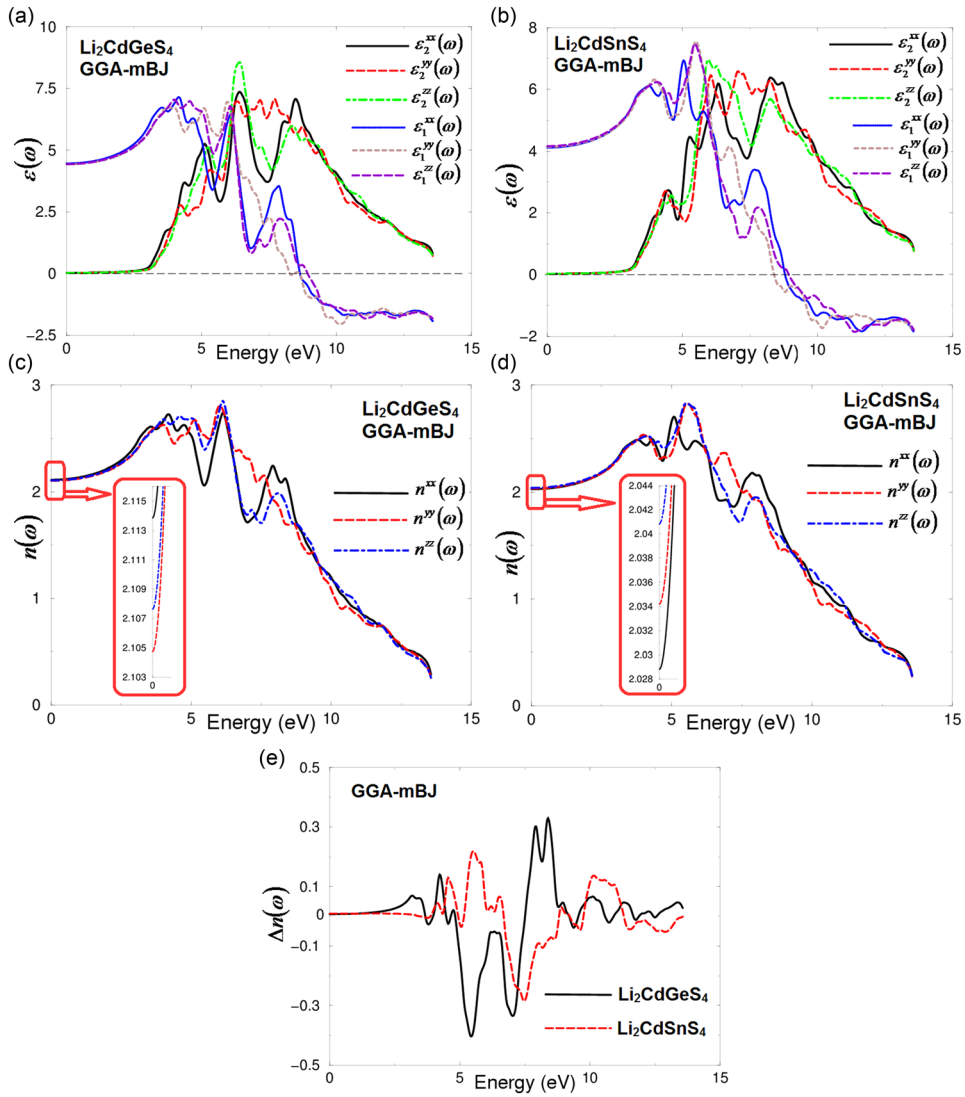

FIG. 5. (a) Calculated $\varepsilon_2^{xx}(\omega)$ (dark solid curve-black), $\varepsilon_2^{yy}(\omega)$ (light long dashed curve-red), and $\varepsilon_2^{zz}(\omega)$ (light dotted dashed curve-green) along with calculated $\varepsilon_1^{xx}(\omega)$ (dark solid curve-blue), $\varepsilon_1^{yy}(\omega)$ (light dashed curve-brown), and $\varepsilon_1^{zz}(\omega)$ (light solid curve-violet) for Li_2CdGeS_4. (b) Calculated $\varepsilon_2^{xx}(\omega)$ (dark solid curve-black), $\varepsilon_2^{yy}(\omega)$ (light long dashed curve-red), and $\varepsilon_2^{zz}(\omega)$ (light dotted dashed curve-green) along with calculated $\varepsilon_1^{xx}(\omega)$ (dark solid curve-blue), $\varepsilon_1^{yy}(\omega)$ (light dashed curve-brown), and $\varepsilon_1^{zz}(\omega)$ (light sold curve-violet) for Li_2CdSnS_4. (c) Calculated refractive indices $n^{xx}(\omega)$ (dark solid curve-black), $n^{yy}(\omega)$ (light dashed curve-red), and $n^{zz}(\omega)$ (light dotted dashed curve-blue) spectrum Li_2CdGeS_4. (d) Calculated refractive indices $n^{xx}(\omega)$ (dark solid curve-black), $n^{yy}(\omega)$ (light dashed curve-red), and $n^{zz}(\omega)$ (light dotted dashed curve-blue) spectrum Li_2CdSnS_4. (e) Calculated birefringence $\Delta n(\omega)$ for Li_2CdGeS_4 (dark solid curve-black) and Li_2CdSnS_4 (light long dashed curve-red).

ionic one.[31] This may be one of the reasons for the strong linear and nonlinear optical properties in Li_2CdGeS_4.

B. Complex first-order linear optical dispersion

Based on the calculated band structure, we can obtain the linear optical properties. The linear optical properties are calculated using the optical code implemented in the WIEN2k package;[28] for more details, please see the user guide[32] and Ref. 33. The optical properties can provide more detailed information about the electronic structure of the materials. It is well-known that the optical properties are very sensitive to the energy band gap. In the DFT, by solving the Kohn-Sham equations, we map an interacting many-body system to a non-interacting hypothetical system which has the same electron density. The price that we will pay is the definition of a new functional that is called the exchange-correlation functional. Unfortunately, the exact form of exchange-correlation functional is unknown. Therefore, the accuracy of our results will be sensitive to selection of the exchange-correlation functional, and it can play a major role in the accuracy of our results, and this is one of the main questions in DFT. Thus, we would like to mention that in our previous works[34–36] we have calculated the energy band gap and the linear and nonlinear optical susceptibilities using the FPLAPW method within mBJ on several systems whose energy band gap, and linear and nonlinear optical susceptibilities are known experimentally; in those previous calculations, we found very good agreement with the experimental data. Thus, we believe that our calculations reported in this paper would produce very

TABLE I. The calculated energy band gap in comparison with the experimental value, $\varepsilon_1^{xx}(0)$, $\varepsilon_1^{yy}(0)$, $\varepsilon_1^{zz}(0)$, $\varepsilon_1^{average}(0)$, $\delta\varepsilon$, ω_p^{xx}, ω_p^{yy}, ω_p^{zz}, $n^{xx}(0)$, $n^{yy}(0)$, $n^{zz}(0)$, and $\Delta n(0)$.

	Li_2CdGeS_4		Li_2CdSnS_4	
	This work	Expt.	This work	Expt.
Eg (eV)	3.10, 2.78[a]	3.15[b]	3.26, 2.50[a]	3.23[b]
$\varepsilon_1^{xx}(0)$	4.468		4.116	
$\varepsilon_1^{yy}(0)$	4.429		4.137	
$\varepsilon_1^{zz}(0)$	4.442		4.164	
$\varepsilon_1^{average}(0)$	4.446		4.139	
$\delta\varepsilon$	−0.00742		−0.00918	
ω_p^{xx}	8.666		8.902	
ω_p^{yy}	8.285		8.421	
ω_p^{zz}	8.938		8.938	
$n^{xx}(0)$	2.113		2.028	
$n^{yy}(0)$	2.104		2.034	
$n^{zz}(0)$	2.107		2.040	
$\Delta n(0)$	+0.009		+0.009	

[a]Reference 19 (other theoretical work).
[b]Reference 14 (experimental work).

accurate and reliable results. Therefore, we have used the mBJ to calculate the electronic band structures and hence the optical properties of Li_2CdGeS_4 and Li_2CdSnS_4. The imaginary part of the linear optical properties $\varepsilon_2^{xx}(\omega)$, $\varepsilon_2^{yy}(\omega)$, and $\varepsilon_2^{zz}(\omega)$ for the orthorhombic system (Li_2CdGeS_4 and Li_2CdSnS_4) is calculated and presented in Figs. 5(a) and 5(b). It has been noticed that substituting Ge by Sn leads to shift the whole spectral structure towards higher energies and lowers the magnitudes of the optical components. The spectral structure of Li_2CdGeS_4 exhibits three main peaks for $\varepsilon_2^{xx}(\omega)$ and $\varepsilon_2^{zz}(\omega)$ components with small humps, while $\varepsilon_2^{yy}(\omega)$ shows one broad peak with two small humps situated on the left shoulder. Whereas Li_2CdSnS_4 exhibits two main peaks for $\varepsilon_2^{xx}(\omega)$, $\varepsilon_2^{yy}(\omega)$, and $\varepsilon_2^{zz}(\omega)$ with several humps situated on the left and right shoulders. The absorption edges occur at 3.10 eV (Li_2CdGeS_4) and 3.23 eV (Li_2CdSnS_4), as shown in Figs. 5(a) and 5(b) and the supplementary material Fig. S1.[37] These absorption edges are originated from the optical transitions between S-3p and Ge-4s/4p (Sn-5s/5p) and Cd-5s/4p states. The optical transitions are calculated from the momentum matrix elements between the occupied and unoccupied bands, giving rise to the selection rules as shown in the supplementary material Fig. S2.[37] Furthermore, the calculated real part of the optical dielectric function can give information about the energy gap, since the calculated static electronic dielectric constant by $\varepsilon_\infty = \varepsilon_1(0)$ is inversely related to the energy gap, this could be explained on the basis of the Penn model.[38] As it is clear that the values of $\varepsilon_1^{xx}(0)$, $\varepsilon_1^{yy}(0)$, and $\varepsilon_1^{zz}(0)$ for Li_2CdGeS_4 are higher than those obtained from Li_2CdSnS_4, hence higher $\varepsilon_1(0)$ exhibits a lower energy gap. This supports our finding that substituting Ge by Sn leads to enlargement of the energy gap. It has been noticed that for the Li_2CdGeS_4 compound $\varepsilon_1^{yy}(0) \approx \varepsilon_1^{zz}(0)$; it represents the parallel component. While for the Li_2CdSnS_4 compound, $\varepsilon_1^{xx}(0) \approx \varepsilon_1^{yy}(0)$ represents the parallel component. The calculated values of $\varepsilon_1^{xx}(0)$, $\varepsilon_1^{yy}(0)$, and $\varepsilon_1^{zz}(0)$ along with the calculated plasmon oscillations ω_p^{xx}, ω_p^{yy}, and ω_p^{zz} for both compounds are presented in Table I. The plasmon oscillations are associated with inter-band transitions that occur at energy where optical spectra of the real part cross zero. The optical components exhibit a considerable anisotropy; this is one of the important features of the optical spectra. The other important feature is the uniaxial anisotropy ($\delta\varepsilon$) which can be obtained from $\varepsilon_1^{xx}(0)$, $\varepsilon_1^{yy}(0)$, $\varepsilon_1^{zz}(0)$, and $\varepsilon_1^{average}(0)$. Following Figs. 5(a) and 5(b), we found that both compounds possess negative $\delta\varepsilon$, as shown in Table I.

The calculated refractive indices of Li_2CdGeS_4 and Li_2CdSnS_4 as derived from the complex dielectric function are presented in Figs. 5(c) and 5(d). It has been noticed that for Li_2CdGeS_4 compounds, $n^{yy}(0) \approx n^{zz}(0) = n_o(0)$ represents the parallel component ($n^{\Pi}(0)$), whereas $n^{xx}(0)$ is the perpendicular one ($n^{\perp}(0) = n_e(0)$). While Li_2CdSnS_4 compounds show that $n^{xx}(0) \approx n^{yy}(0)$ as $n_o(0)$ and $n^{zz}(0) = n_e(0) = n^{\perp}(0)$. Thus, the birefringence can be estimated from $\Delta n(\omega) = n_e(\omega) - n_o(\omega)$. It has been found that both compounds exhibit positive birefringence at the static limit, as shown in Table I. We found that the $\Delta n(0)$ for $Li_2CdGeS_4 > Li_2CdSnS_4$; hence, Li_2CdSnS_4 exhibits weaker anisotropy. The birefringence is necessary to fulfil the phase-matching condition. Therefore, we expected Li_2CdGeS_4 to produce higher second harmonic generation than Li_2CdSnS_4. The dispersion of the birefringence of the two compounds is illustrated in Fig. 5(e).

C. Complex second-order non-linear optical dispersion

To achieve accurate results for the calculated nonlinear optical properties, an accurate energy band gap is required, since the band gap value comes in the denominator of the complex nonlinear optical formulas which are used to calculate the complex nonlinear optical. These formulas are presented elsewhere.[39–42] The nonlinear optical properties are calculated using the NLO code, which is compatible with the WIEN2k package, see Refs. 39 and 40. Therefore, to achieve accurate results, we have applied the mBJ, which allows the calculation of the band gap with accuracy similar to the very expensive GW calculations.[30] Moreover, a quasi-particle self-energy correction at the level of scissors operators is applied to avoid the DFT drawback, since the calculated energy gap is still less than the measured one by around 0.05 eV for Li_2CdGeS_4 and 0.06 eV for Li_2CdSnS_4. In the scissors operators, the energy bands are rigidly shifted to merely bring the calculated energy gap to the exact experimental value. The orthorhombic symmetry allows seven non-zero tensor components $\chi^{(2)}_{113}(-2\omega;\omega;\omega) = \chi^{(2)}_{131}(-2\omega;\omega;\omega)$, $\chi^{(2)}_{223}(-2\omega;\omega;\omega) = \chi^{(2)}_{232}(-2\omega;\omega;\omega)$, $\chi^{(2)}_{311}(-2\omega;\omega;\omega)$, $\chi^{(2)}_{322}(-2\omega;\omega;\omega)$, and $\chi^{(2)}_{333}(-2\omega;\omega;\omega)$; two of them are equal, thus only five non-zero tensor components can be considered. One of those five tensors is considered to be the dominant one. Figs. 6(a) and 6(b) show the calculated absolute value $|\chi^{(2)}_{ijk}(-2\omega;\omega;\omega)|$ of those five tensors. It has been noticed that $|\chi^{(2)}_{333}(-2\omega;\omega;\omega)|$ is the dominant one, since it shows the highest value among the others, as shown in Tables II and III. Following these tables, we can see that Li_2CdGeS_4

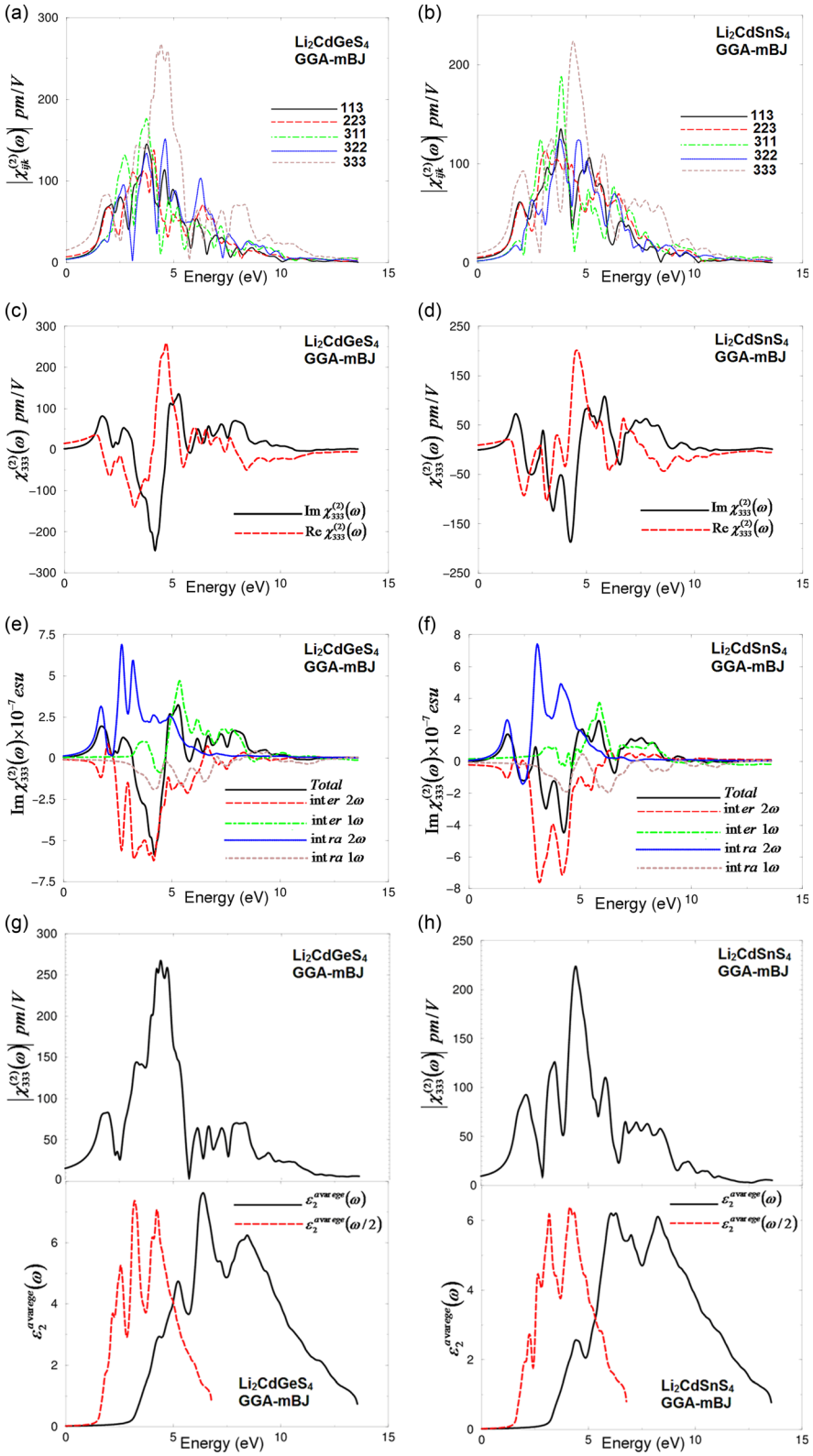

FIG. 6. (a) Calculated $|\chi^{(2)}_{ijk}(\omega)|$ for the five tensor components of Li_2CdGeS_4. (b) Calculated $|\chi^{(2)}_{ijk}(\omega)|$ for the five tensor components of Li_2CdSnS_4. (c) Calculated imaginary $\chi^{(2)}_{333}(\omega)$(dark solid curve-black) and real $\chi^{(2)}_{333}(\omega)$ (light dashed curve-red) spectra of Li_2CdGeS_4. (d) Calculated imaginary $\chi^{(2)}_{333}(\omega)$(dark solid curve-black) and real $\chi^{(2)}_{333}(\omega)$ (light dashed curve-red) spectra of Li_2CdSnS_4. (e) Calculated total Im $\chi^{(2)}_{333}(\omega)$ spectrum (dark solid curve-black) along with the intra $(2\omega)/(1\omega)$ (light solid curve-blue)/(light dashed dotted curve-cyan) and inter $(2\omega)/(1\omega)$ (light long dashed curve-red)/(light dotted curve-green)-band contributions of Li_2CdGeS_4, here all Im $\chi^{(2)}_{222}(\omega)$ are multiplied by 10^{-7}, in esu units. (f) Calculated total Im $\chi^{(2)}_{333}(\omega)$ spectrum (dark solid curve-black) along with the intra $(2\omega)/(1\omega)$ (light solid curve-blue)/(light dashed dotted curve-cyan) and inter $(2\ \omega)/(1\ \omega)$ (light long dashed curve-red)/(light dotted curve-green)-band contributions of Li_2CdSnS_4, here all Im $\chi^{(2)}_{222}(\omega)$ are multiplied by 10^{-7}, in esu units. (g) Upper panel—calculated $|\chi^{(2)}_{333}(\omega)|$ (dark solid curve-black); lower panel—calculated $\varepsilon_2^{xx}(\omega)$ (dark solid curve-black) and calculated $\varepsilon_2^{xx}(\omega/2)$ (dark dashed curve-red) of Li_2CdGeS_4. (h) Upper panel—calculated $|\chi^{(2)}_{333}(\omega)|$ (dark solid curve-black); lower panel—calculated $\varepsilon_2^{xx}(\omega)$ (dark solid curve-black) and calculated $\varepsilon_2^{xx}(\omega/2)$ (dark dashed curve-red) of Li_2CdSnS_4.

exhibits larger SHG than that of Li_2CdSnS_4 and very close to the experimental value of the well-known $KTiOPO_4$ (KTP) single crystals, which exhibits a SHG value of about 16.9,[43] 13.7,[44] 15.4 ± 0.2,[45] 14.6 ± 1.0,[46] 17.4 ± 1.7,[47] 16.9 ± 3.3,[48] 16.9 ± 1.7,[49] 10.6 ± 7.5,[50] 16.75,[51] and 16.65.[51]

The real and imaginary parts of $\chi^{(2)}_{333}(-2\omega;\omega;\omega)$ are presented in Figs. 6(c) and 6(d) for Li_2CdGeS_4 and Li_2CdSnS_4. These figures show that the Im $\chi^{(2)}_{333}(-2\omega;\omega;\omega)$ value rises at a half value of the energy band gap due to 2 ω terms oscillation, then at the exact value of the fundamental gap the ω terms start to oscillate to be added to 2ω terms. While in the higher energies, only ω terms will contribute. To analyze the spectral features of the Im $\chi^{(2)}_{333}(-2\omega;\omega;\omega)$, we have calculated the $2\omega/\omega$ inter-/intra-band contributions in order to understand the origin of the strong second harmonic generation of the dominant component. These are shown in Figs. 6(e) and

TABLE II. Calculated $|\chi^{(2)}_{ijk}(\omega)|$ and β_{ijk} of Li_2CdGeS_4, in pm/V at static limit and at $\lambda = 1064$ nm, in comparison with the experimental value of the well known $KTiOPO_4$ (KTP) single crystals, which exhibits a SHG value of about 16.9,[43] 13.7,[44] 15.4 ± 0.2,[45] 14.6 ± 1.0,[46] 17.4 ± 1.7,[47] 16.9 ± 3.3,[48] 16.9 ± 1.7,[49] 10.6 ± 7.5,[50] 16.75,[51] and 16.65 (Ref. 51) at $\lambda = 1064$. Where 1 pm/V = 2.387×10^{-9} esu. The bold are the values of the dominate component.

Li_2CdGeS_4				
Tensor components	$\chi^{(2)}_{ijk}(0)$	Theory $d_{ijk} = 0.5\ \chi^{(2)}_{ijk}(\omega)$	$\chi^{(2)}_{ijk}(\omega)$ at $\lambda = 1064$	Theory $d_{ijk} = 0.5\ \chi^{(2)}_{ijk}(\omega)$
$\lvert\chi^{(2)}_{113}(\omega)\rvert$	4.538	$d_{15} = 2.269$	15.409	$d_{15} = 7.704$
$\lvert\chi^{(2)}_{223}(\omega)\rvert$	7.144	$d_{24} = 3.572$	17.527	$d_{24} = 8.763$
$\lvert\chi^{(2)}_{311}(\omega)\rvert$	4.269	$d_{31} = 2.134$	12.583	$d_{31} = 6.291$
$\lvert\chi^{(2)}_{322}(\omega)\rvert$	3.932	$d_{32} = 1.966$	11.879	$d_{32} = 5.939$
$\lvert\chi^{(2)}_{333}(\omega)\rvert$	**15.288**	$\boldsymbol{d_{33} = 7.644}$	**37.297**	$\boldsymbol{d_{33} = 18.648}$
β_{333}	$\mathbf{5.601 \times 10^{-30}}$ **esu**		$\mathbf{13.015 \times 10^{-30}}$ **esu**	

TABLE III. Calculated $|\chi^{(2)}_{ijk}(\omega)|$ and β_{ijk} of Li_2CdSnS_4, in pm/V at static limit and at $\lambda = 1064$ nm, in comparison with the experimental value of the well known $KTiOPO_4$ (KTP) single crystals, which exhibits a SHG value of about 16.9,[43] 13.7,[44] 15.4 ± 0.2,[45] 14.6 ± 1.0,[46] 17.4 ± 1.7,[47] 16.9 ± 3.3,[48] 16.9 ± 1.7,[49] 10.6 ± 7.5,[50] 16.75,[51] and 16.65 (Ref. 51) at $\lambda = 1064$. Where 1 pm/V = 2.387×10^{-9} esu. The bold are the values of the dominate component.

Li_2CdSnS_4				
Tensor components	$\chi^{(2)}_{ijk}(0)$	Theory $d_{ijk} = 0.5\ \chi^{(2)}_{ijk}(\omega)$	$\chi^{(2)}_{ijk}(\omega)$ at $\lambda = 1064$	Theory $d_{ijk} = 0.5\ \chi^{(2)}_{ijk}(\omega)$
$\lvert\chi^{(2)}_{113}(\omega)\rvert$	4.442	$d_{15} = 2.221$	13.269	$d_{15} = 6.634$
$\lvert\chi^{(2)}_{223}(\omega)\rvert$	5.700	$d_{24} = 2.850$	13.928	$d_{24} = 6.964$
$\lvert\chi^{(2)}_{311}(\omega)\rvert$	1.918	$d_{31} = 0.959$	7.714	$d_{31} = 3.857$
$\lvert\chi^{(2)}_{322}(\omega)\rvert$	1.933	$d_{32} = 0.966$	7.338	$d_{32} = 3.669$
$\lvert\chi^{(2)}_{333}(\omega)\rvert$	**9.569**	$\boldsymbol{d_{33} = 4.784}$	**25.507**	$\boldsymbol{d_{33} = 12.753}$
β_{333}	$\mathbf{3.737 \times 10^{-30}}$ **esu**		$\mathbf{9.704 \times 10^{-30}}$ **esu**	

6(f). Furthermore, the spectral structure of the dominant component can be associated with the absorptive part of the corresponding dielectric function $\varepsilon_2(\omega)$ as a function of both $\omega/2$ and ω, to identify the origin of the spectral peaks as caused by $2\omega/\omega$ inter-/intra-band contributions, as shown in Figs. 6(g) and 6(h). The first structure in $|\chi^{(2)}_{333}(\omega)|$ between 1.57 and 3.15 eV (1.63 and 3.26 eV) for Li_2CdGeS_4 (Li_2CdSnS_4) is mainly originated from 2 ω resonance [see $\varepsilon_2(\omega/2)$, Figs. 6(g) and 6(h)—lower panel]. The second structure between 3.15 and 5.0 eV (3.26 and 5.0 eV) is associated with interference between 2 ω and ω resonances (the threshold of $\varepsilon_2(\omega)$) [see $\varepsilon_2(\omega/2)$ and $\varepsilon_2(\omega)$, Figs. 6(g) and 6(h)—lower panel]. The last spectral structure from 5.0 and above is mainly due to ω resonance and is associated with the second structure in $\varepsilon_2(\omega)$. With the aid of the existing values of the SHG for the dominant components of Li_2CdGeS_4 and Li_2CdSnS_4, we obtained the values of the microscopic first hyperpolarizability, β_{333},[50] the vector component along the dipole moment direction, at the static limit and at $\lambda = 1064$ nm. These values are listed in Tables II and III. In general, the microscopic first hyperpolarizability term, β_{ijk}, cumulatively yields a bulk observable second order susceptibility term, $\chi^{(2)}_{ijk}(\omega)$, which in turn is responsible for the high SHG response.[22,23]

IV. CONCLUSIONS

The influence of replacing Ge by Sn on the electronic band structures and the linear and nonlinear optical susceptibilities were investigated by means of DFT. The all-electron FP-LAPW + lo method was used. Using PBE-GGA, the experimental geometries of Li_2CdGeS_4 and Li_2CdSnS_4 were optimized by minimizing the forces acting on the atoms. The resulting geometries were used to calculate the electronic band structure, the density of states, the electronic charge density, and the linear and nonlinear optical susceptibilities using the PBE-GGA and the mBJ. It has been found that the mBJ succeeds by a large amount in bringing the calculated energy gap closer to the experimental one. The electronic band structure shows the direct band nature of the investigated compounds, and the PDOS reveals the roles of the orbitals. The valence electronic charge density exhibits a clear visualization to understand the origin of bonding characters. The considerable anisotropy in the linear optical properties, the presence of polarizable M-S bonding, and the wide energy gap causes in Li_2CdGeS_4 and Li_2CdSnS_4 compounds to exhibit strong SHG and exceptional laser damage thresholds. It has been found that Li_2CdGeS_4 exhibits higher SHG than that of Li_2CdSeS_4. The resulting SHG is comparable to that of the well-known KTP single crystals.

ACKNOWLEDGMENTS

The result was developed within the CENTEM project, Reg. No. CZ.1.05/2.1.00/03.0088, cofunded by the ERDF as part of the Ministry of Education, Youth and Sports OP RDI programme and, in the follow-up sustainability stage, supported through CENTEM PLUS (LO1402) by financial means from the Ministry of Education, Youth and Sports under the "National Sustainability Programme I." Computational resources were provided by MetaCentrum (LM2010005) and CERIT-SC (CZ.1.05/3.2.00/08.0144) infrastructures.

[1]J. Zhang, Z. Zhang, W. Zhang, Q. Zheng, Y. Sun, C. Zhang, and X. Tao, "Polymorphism of $BaTeMo_2O_9$: A new polar polymorph and the phase transformation," Chem. Mater. **23**, 3752–3761 (2011).

[2]V. Kapustianyk, B. Turko, A. Kostruba, Z. Sofiani, B. Derkowska, S. Dabos-Seignon, B. Barwinski, Yu. Eliyashevskyi, and B. Sahraoui, "Influence of size effect and sputtering conditions on the crystallinity and optical properties of ZnO thin films," Opt. Commun. **269**, 346–350 (2007).

[3]S. Zongo, A. P. Kerasidou, B. T. Sone, A. Diallo, P. Mthunzi, K. Iliopoulos, M. Nkosi, M. Maaza, and B. Sahraoui, "Nonlinear optical properties of poly(methyl methacrylate) thin films doped with Bixa Orellana dye," Appl. Surf. Sci. **340**, 72–77 (2015).

[4]J. Niziol, W. Baran, E. Gondek, I. V. Kityk, A. Mendys, M. Zylewski, and A. H. Reshak, "Synthesis and NLO properties of new chromophores based on Imidazo[1,2-A]Pyridine," Chem. Eng. Commun. **196**, 1466–1474 (2009).

[5]A. Majchrowski, E. Gondek, K. Ozga, I. V. Kityk, A. H. Reshak, and T. Łukasiewicz, "Photoinduced nonlinear optical effects in the Pr doped BiB_3O_6 glass nanoparticles incorporated into the polymer matrices," J. Alloys Compd. **485**, 29–32 (2009).

[6]Z. L. Gao, Q. Wu, X. T. Liu, Y. X. Sun, and X. T. Tao, "Biaxial crystal α-BaTeMo2O9: Theory study of large birefringence and wide-band polarized prisms design," Opt. Express **23**, 3851–3860 (2015).

[7]I. Fuks-Janczarek, J. Luc, B. Sahraoui, F. Dumur, P. Hudhomme, J. Berdowski, and I. V. Kityk, "Third-order nonlinear optical figure of merits for conjugated TTF-quinone molecules," J. Phys. Chem. B **109**(20), 10179–10183 (2005).

[8]I. Fuks-Janczarek, S. Dabos-Seignon, B. Sahraoui, I. V. Kityk, J. Berdowski, E. Allard, and J. Cousseau, "Experimental study of third-order nonlinear optical properties in C60-TTF dyads with saturated (-C-C-) chemical bonds," Opt. Commun. **211**(1–6), 303–308 (2002).

[9]N. A. Goryunova, in *The Chemistry of Diamond-Like Semiconductors*, edited by J. C. Anderson (The MIT Press, Cambridge, U.K., 1965).

[10]E. Parthe, *Crystal Chemistry of Tetrahedral Structures* (Gordon and Breach Science Publishers, New York, 1964).

[11]E. Parthe, K. Yvon, and R. H. Dietch, "The crystal structure of Cu_2CdGeS_4 and other quaternary normal tetrahedral structure compounds," Acta Crystallogr., Sect. B **25**, 1164–1174 (1969).

[12]D. M. Schleich and A. Wold, "Optical and electrical properties of quaternary chalcogenides," Mater. Res. Bull. **12**, 111–114 (1977).

[13]M. Quintero, A. Barreto, P. Grima, R. Tovar, E. Quintero, G. S. Porras, J. Ruiz, J. C. Woolley, G. Lamarche, and A. M. Lamarche, "Crystallographic properties of I_2–Fe–iv–vi_4 magnetic semiconductor compounds," Mater. Res. Bull. **34**, 2263–2270 (1999).

[14]J. W. Lekse, M. A. Moreau, K. L. McNerny, J. Yeon, P. S. Halasyamani, and J. A. Aitken, "Second-harmonic generation and crystal structure of the diamond-like semiconductors Li_2CdGeS_4 and Li_2CdSnS_4," Inorg. Chem. **48**, 7516–7518 (2009).

[15]A. G. Jackson, M. C. Ohmer, and S. R. LeClair, "Relationship of the second order nonlinear optical coefficient to energy gap in inorganic non-centrosymmetric crystals," Infrared Phys. Technol. **38**, 233–244 (1997).

[16]A. H. Reshak and S. Auluck, "The linear and nonlinear optical properties of WS_xSe_{2-x} (x = 0.5, 1.5, and 2.0)," Physica B **393**, 88–93 (2007).

[17]J. I. Jang, D. J. Clark, J. A. Brant, J. A. Aitken, and Y. S. Kim, "Highly efficient infrared optical nonlinearity of a wide-bandgap chalcogenide Li_2CdGeS_4," Opt. Lett. **39**, 4579–4582 (2014).

[18]J. A. Brant, D. J. Clark, Y. S. Kim, J. I. Jang, J.-H. Zhang, and J. A. Aitken, "Li_2CdGeS_4, a diamond-like semiconductor with strong second-order optical nonlinearity in the infrared and exceptional laser damage threshold," Chem. Mater. **26**, 3045–3048 (2014).

[19]Y. Li, W. Fan, H. Sun, X. Cheng, P. Li, and X. Zhao, "Electronic, optical and lattice dynamic properties of the novel diamond-like semiconductors Li_2CdGeS_4 and Li_2CdSnS_4," J. Phys.: Condens. Matter **23**, 225401 (2011).

[20]W. Peng, X. Li, and J. Du, "First principles investigations on structural, elastic, electronic, and optical properties of Li_2CdGeS_4," Mater. Trans. **54**, 2167–2172 (2013).

[21]X. Li, W. Peng, and H. Fu, "Theoretical investigations on the elastic, electronic and thermal properties of orthorhombic Li_2CdGeS_4 under pressure," J. Alloys Compd. **581**, 867–872 (2013).

[22]R. W. Boyd, *Nonlinear Optics*, 3rd ed. (Academic Press is an imprint of Elsevier, 2008), ISBN: 978-0-12-369470-6.

[23]W. T. A. Harrison, M. L. F. Phillips, and G. D. Stucky, "Substitution chemistry of gallium for titanium in nonlinear optical $KTiOPO_4$: Syntheses and single-crystal structures of KGaF1-.delta.(OH).delta.PO_4 (.delta.apprxeq. 0.3) and $KGa_{0.5}Ge_{0.5}(F,OH)_{0.5}PO_4$," Chem. Mater. **7**, 1849–1856 (1995).

[24]J. Zhang, X. F. Li, and K. L. Yao, "First-principles study of the ferroelectric and optical properties of $BaTeMo_2O_9$," J. Alloys Compd. **509**, 4929–4934 (2011).

[25]G. E. Davydyuk, O. Y. Khyzhun, A. H. Reshak, H. Kamarudin, G. L. Myronchuk, S. P. Danylchuk, A. O. Fedorchuk, L. V. Piskach, M. Yu. Mozolyuk, and O. V. Parasyuk, "Photoelectrical properties and the electronic structure of $Tl_{1-x}In_{1-x}Sn_xSe_2$ ($x = 0$, 0.1, 0.2, 0.25) single crystalline alloys," Phys. Chem. Chem. Phys. **15**, 6965 (2013).

[26]A. H. Reshak, Y. M. Kogut, A. O. Fedorchuk, O. V. Zamuruyeva, G. L. Myronchuk, O. V. Parasyuk, H. Kamarudin, S. Auluck, K. J. Plucinskig, and J. Bila, "Linear, non-linear optical susceptibilities and the hyperpolarizability of the mixed crystals $Ag_{0.5}Pb_{1.75}Ge(S_{1-x}Se_x)_4$: Experiment and theory," J. Phys. Chem. Chem. Phys. **15**, 18979–18986 (2013).

[27]V. I. Gavrilenko, "Ab initio theory of second harmonic generation from semiconductor surfaces and interfaces," Phys. Status Solidi A **188**, 1267–1280 (2001).

[28]P. Blaha, K. Schwarz, G. K. H. Madsen, D. Kvasnicka, and J. Luitz, "WIEN2k, an augmented plane wave plus local orbitals program for calculating crystal properties," Vienna University of Technology, Austria (2001).

[29]J. P. Perdew, K. Burke, and M. Ernzerhof, "Generalized gradient approximation made simple," Phys. Rev. Lett. **77**, 3865–3868 (1996).

[30]F. Tran and P. Blaha, "Accurate band gaps of semiconductors and insulators with a semilocal exchange-correlation potential," Phys. Rev. Lett. **102**, 226401 (2009).

[31]F. Wu, H. Z. Song, J. F. Jia, and X. Hu, "Effects of Ce, Y, and Sm doping on the thermoelectric properties of Bi_2Te_3 alloy," Prog. Nat. Sci. **23**, 408–412 (2013).

[32]See http://www.wien2k.at/reg_user/textbooks/usersguide.pdf for the optic code WIEN2k user guide.

[33]C. Ambrosch-Draxl and J. O. Sofo, "Linear optical properties of solids within the full-potential linearized augmented planewave method," Comput. Phys. Commun. **175**, 1–14 (2006).

[34]A. H. Reshak, "Specific features of electronic structures and optical susceptibilities of molybdenum oxide," RSC Adv. **5**, 22044 (2015).

[35]A. H. Reshak, H. Huang, H. Kamarudin, and S. Auluck, "Alkali-metal/alkaline-earth-metal fluorine beryllium borate $NaSr_3Be_3B_3O_9F_4$ with large nonlinear optical properties in the deep-ultraviolet region," J. Appl. Phys. **117**, 085703 (2015).

[36]A. H. Reshak, "Transport properties of g-BC3 and t-BC3 phases," RSC Adv. **5**, 33632–33638 (2015).

[37]See supplementary material at http://dx.doi.org/10.1063/1.4943100 for Fig. S1: (a) The calculated electronic band structure of Li_2CdGeS_4 compound in the energy region between the Fermi level and 4.0 eV in comparison with the measured absorption edges taken from Ref. 14, we have used special software to extract the data from Figure 4 of Ref. 14, then we re-plot the absorption vs electronic band structure. (b) The calculated electronic band structure of Li_2CdSnS_4 compound in the energy region between the Fermi level and 4.0 eV in comparison with the measured absorption edges taken from Ref. 14, we have used special software to extract the data from Figure 4 of Ref. 14, then we re-plot the absorption vs electronic band structure. Fig. S2: (a) The optical transitions depicted on a generic band structure of Li_2CdGeS_4 compound. For simplicity, we have labeled the optical transitions as A, B, and C. The transitions (A) are responsible for the structures for $\varepsilon_2^{xx}(\omega)$, $\varepsilon_2^{yy}(\omega)$, and $\varepsilon_2^{zz}(\omega)$ in the spectral range 0.0–5.0 eV; the transitions (B) 5.0–10.0 eV, and the transitions (C) 10.0–14.0 eV. (b) The optical transitions depicted on a generic band structure of Li_2CdSnS_4 compound. For simplicity, we have labeled the optical transitions as A, B, and C. The transitions (A) are responsible for the structures for $\varepsilon_2^{xx}(\omega)$, $\varepsilon_2^{yy}(\omega)$, and $\varepsilon_2^{zz}(\omega)$ in the spectral range 0.0–5.0 eV; the transitions (B) 5.0–10.0 eV, and the transitions (C) 10.0–14.0 eV.

[38]D. R. Penn, "Wave-number-dependent dielectric function of semiconductors," Phys. Rev. B **128**, 2093 (1962).

[39]S. Sharma and C. Ambrosch-Draxl, "Second-harmonic optical response from first principles," Phys. Scr. T **109**, 128 (2004).

[40]S. Sharma, J. K. Dewhurst, and C. Ambrosch-Draxl, "Linear and second-order optical response of III-V monolayer superlattices," Phys. Rev. B **67**, 165332 (2003).

[41]S. N. Rashkeev, W. R. L. Lambrecht, and B. Segall, "Efficient ab initio method for the calculation of frequency-dependent second-order optical response in semiconductors," Phys. Rev. B **57**, 3905 (1998).

[42]J. L. P. Hughes and J. E. Sipe, "Calculation of second-order optical response in semiconductors," Phys. Rev. B **53**, 10751 (1996).

[43]K. Zhang and X. Wang, "Structure sensitive properties of KTP-type crystals," Chin. Sci. Bull. **46**, 2028–2036 (2001).
[44]See http://www.castech-us.com/casktp.htm for the experimental value of the SHG of KTP crystal.
[45]M. V. Pack, D. J. Armstrong, and A. V. Smith, "Measurement of the $\chi^{(2)}$ tensors of $KTiOPO_4$, $KTiOAsO_4$, $RbTiOPO_4$, and $RbTiOAsO_4$ crystals," Appl. Opt. **43**, 3319 (2004).
[46]I. Shoji, T. Kondo, A. Kitamoto, M. Shirane, and R. Ito, "Absolute scale of second-order nonlinear-optical coefficients," J. Opt. Soc. Am. B **14**, 2268 (1997).
[47]A. Anema and T. Rasing, "Relative signs of the nonlinear coefficients of potassium titanyl phosphate," Appl. Opt. **36**, 5902 (1997).
[48]L. K. Cheng, L. T. Cheng, J. Galperin, P. A. M. Hotsenpiller, and J. D. Bierlein, "Crystal growth and characterization of $KTiOPO_4$ isomorphs from the self-fluxes," J. Cryst. Growth **137**, 107–115 (1994).
[49]H. Vanherzeele and J. D. Bierlein, "Magnitude of the nonlinear-optical coefficients of $KTiOPO_4$," Opt. Lett. **17**, 982–984 (1992).
[50]B. Boulanger, J. P. Feve, G. Marnier, and B. Menaert, "Methodology for optical studies of nonlinear crystals: Application to the isomorph family $KtiOPO_4$, $KTiOAsO_4$, $RbTiOAsO_4$ and $CsTiOAsO_4$," Pure Appl. Opt. **7**, 239 (1998).
[51]A. H. Reshak, I. V. Kityk, and S. Auluck, "Investigation of the linear and nonlinear optical susceptibilities of $KTiOPO_4$ single crystals: Theory and experiment," J. Phys. Chem. B **114**, 16705–16712 (2010).